Soil Salinity Characterization Using Polarimetric InSAR Coherence: Case Studies in Tunisia and Morocco

Meriem Barbouchi, Riadh Abdelfattah, *Senior Member*, *IEEE*, Karem Chokmani, Nadhira Ben Aissa, Rachid Lhissou, and Abderrazzak El Harti

***Abstract*—The phenomenon of soil salinization in semi-arid regions is getting amplified and accentuated by both anthropogenic practices and climate change. Land salinization mapping and monitoring using conventional strategies are insufficient and difficult. Our work aims to study the potential of synthetic aperture radar (SAR) for mapping and monitoring of the spatio-temporal dynamics of soil salinity using interferometry. Our contribution in this paper consists of a statistical relationship that we establish between field salinity measurement and InSAR coherence based on an empirical analysis. For experimental validation, two sites were selected: 1) the region of Mahdia (central Tunisia) and 2) the plain of Tadla (central Morocco). Both sites underwent three ground campaigns simultaneously with three Radarsat-2 SAR image acquisitions. The results show that it is possible to estimate the temporal change in soil electrical conductivity (EC) from SAR images through the InSAR technique. It has been shown that the radar signal is more sensitive to soil salinity in HH polarization using a small incidence angle. However, for the HV polarization, a large angle of incidence is more suitable. This is, under considering the minimal influence of roughness and moisture surfaces, for a given InSAR coherence.**

***Index Terms*—Electrical conductivity (EC), interferometric synthetic aperture radar (InSAR) coherence, polarimetric synthetic aperture radar (SAR), soil salinity.**

I. Introduction

SALINIZATION can be divided into primary and secondary depending on its origin. The first is natural and affects approximately 80% of lands. The second is induced by anthropogenic activities, mainly irrigation [1]. Salinization poses a real threat to the world food security. Indeed, salinization already has affected 400 million hectares, and an equivalent area is threatened by this problem [2]. Tunisia and Morocco, two countries located in arid and semi-arid climate zones, are threatened by ground salinization. More than 8% and 5% of Tunisian and Moroccan areas are already affected by salinity to various degrees [3], respectively. Salinization is characterized by its spatio-temporal evolution. Traditional methods of monitoring its development (analysis in the laboratory, *in situ*) are insufficient and unsuitable due to the speed with which this phenomenon evolves. Therefore, exploration of faster and more reliable methods of investigation is imperative. Many techniques based on remote sensing data such as radar and optical techniques are frequently used in the mapping and monitoring of soil salinity evolution. However, optical remote sensing outputs remain difficult to exploit because of the presence of the cloud layer and dependence on the sun's rays [4], [5].

Radar imagery can provide as a reliable tool for detecting temporal changes in soil salinity regardless of the weather (clouds and rain) and temporal (day–night) conditions [6]–[8]. For agricultural soil, the radar signal is dependent mainly on surface parameters [9], [10]. For example, soil salinity, coupled with moisture (the presence of salt in solution), influences the dielectric properties of soil and consequently the radar signal [11], [12]. Several studies have been conducted on the potential of radar remote sensing in moisture and soil roughness estimation [11], [13], [8], [14]–[17]. Research on salinization is less abundant, although a few studies have been conducted [18]–[20]. Radar interferometry is also used for detecting surface soil changes such as tectonic movement, earthquakes, and desertification [21]. In this study, we use the interferometric coherence as a technique for detecting changes of soil surface characteristics; we then correlate those changes with variation in soil salinity. The main objective is to develop an empirical model that takes into account acquisition parameters like incidence angle and polarization to estimate soil salinity variation based on interferometric coherence. This work aims to explore the capacity of synthetic aperture radar (SAR) for the detection of spatio-temporal variation of soil salinity through electrical conductivity (EC) variation (imaginary part), which is considered as the only quantifiable indicator of soil salinity. For this study, two areas characterized by their different conditions were selected: 1) the

Manuscript received November 29, 2013; revised April 06, 2014; accepted June 11, 2014. Date of publication August 11, 2014; date of current version September 12, 2015.

M. Barbouchi is with the National Agronomic Institute of Tunisia (INAT), Tunis 2083, Tunisia, and also with the COSIM Lab, Higher School of Communications of Tunis, Tunis 2083, Tunisia (e-mail: barbouchi.meriem@yahoo.fr).

R. Abdelfattah is with the COSIM Lab, Higher School of Communications of Tunis, Tunis 2083, Tunisia, and also with the ITI Department, Telecom Bretagne, Telecom Institute, Brest 29200, France (e-mail: riadh.abdelfattah@supcom.rnu.tn).

K. Chokmani is with the Centre Eau Terre Environnement, Institut National de la Recherche Scientifique (INRS), Montreal, QC J3X 1P7, Canada (e-mail: karem.chokmani@ete.inrs.ca).

N. Ben Aissa is with the National Agronomic Institute of Tunisia (INAT), Tunis 2083, Tunisia.

R. Lhissou and A. El Harti are with the Faculty of Science and Technology, University Sultan Moulay Slimane, Beni-Mellal 23000, Morocco (e-mail: rachid.lhissou@gmail.com).

Color versions of one or more of the figures in this paper are available online at http://ieeexplore.ieee.org.

Digital Object Identifier 10.1109/JSTARS.2014.2333535

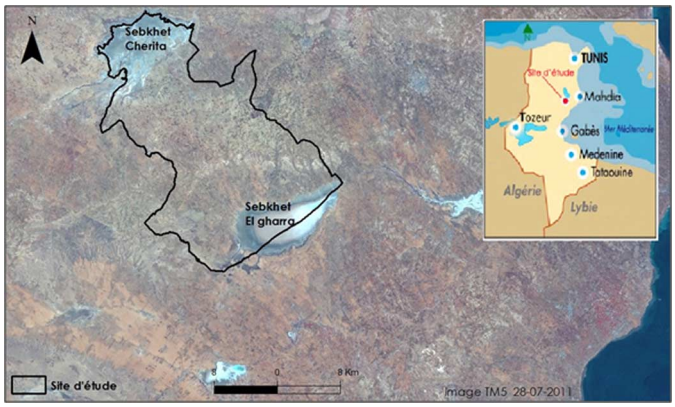

Fig. 1. Location map of the Tunisian site.

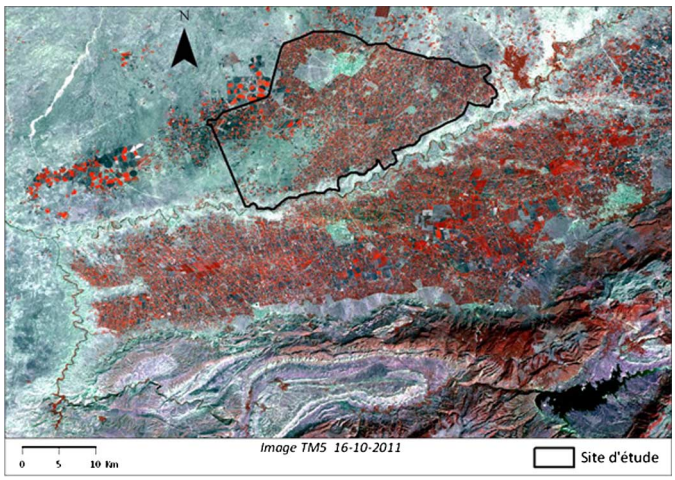

Fig. 2. Location map of the Moroccan site.

first area is in an irrigated region with secondary salinization, located in the plain of Tadla (Morocco), and 2) the second area is in Mahdia region (Tunisia), which is characterized by primary salinization.

II. Study Area and Data Used

Test sites were established in two study areas in the semi-arid bioclimatic zone that suffer from salinization: 1) the governorate of Mahdia in Tunisia and 2) the plain of Tadla in Morocco (Figs. 1 and 2). The sites were chosen in order to test locations with differing origins of salinization and study area characteristics. The Tunisian site is characterized by bare soil, with no agricultural activity except some olive trees grown without irrigation. In this site, salinization is due to natural factors such as climate conditions (average annual evaporation is 1700 mm). Water loss due to evaporation exceeds the contributions by rain, leading to a deficit in water balance [22]. As a result, the presence of saline groundwater induces soil salinization by capillary rise. On the Moroccan site, characterized by agricultural activities, salinization is caused by farming practices such as irrigation with brackish water (1.3 g/l) and excessive use of fertilizer and plant protection products. The Tunisian site belongs to the governorate of Mahdia in central Tunisia. It is located between $10°24'03.39''$E and $10°31'36.65''$E longitude and $35°36'33.08''$N and $35°06'33.97''$N latitude. A location map of this study area is given in Fig. 1. This test site extends between Sebkhat (salt lake) el Ghorra and Sebkhat Echrita. The soils of the Tunisian site are affected by primary salinity due to their closeness to the Sebkhas and the ascent of groundwater. The Moroccan site is the agricultural plain of Tadla, located between $6°51'49.1''$W and $6°30'46.85''$W longitude and $32°19'40.39''$N and $32°32'44.41''$N latitude (Fig. 2). It is irrigated by water collected by the Ahmed El-Hansali dam. The soil of the Moroccan site is characterized by secondary salinization induced by irrigation. In this study, we used eight SAR images of the Tunisian site and nine of the Moroccan site acquired in September, October, and November 2011 by the Radarsat2 satellite. The images were acquired in "Fine Quad Pol" mode, which corresponds to a swath of 25 km $\times$ 25 km and a spatial resolution of 8 m. The incidence angle of acquisitions varied from $25°$ to $46°$. An interferometric pair is created from two images acquired in a configuration of identical acquisition (frame, mode of incidence; Table I).

III. Methodology

A two-phase approach was adopted for modeling and monitoring of soil salinity: the first is the phase, preprocessing, involved georeferencing the SAR images and determining the EC of the sites *in situ*. The second phase focused on the modeling of EC according to coherence (Fig. 3). The following section describes these two steps.

A. EC Determination In Situ

Soil samples were collected throughout each study site during three field campaigns. For the Moroccan site, the first campaign was held on September 27 and 28, 2011, with 38 samples collected (Fig. 4). This campaign was conducted during a dry period, when the salt dynamics were low compared to the wet period, which is characterized by significant redistribution of salts. The second took place on October 24, 2011, with 24 samples. The last took place on November 17, 2011, with 24 samples. In total, 86 samples were collected (Fig. 4). For the Tunisian site, the first campaign was conducted on September 26, 2011, with 17 samples collected (Fig. 5). The second took place on October 24, 2011, with 17 samples. The third was completed on November 17, 2011, with 17 again collected. All sampling points were located by geographical positioning system (GPS) to enable use of the same points in subsequent campaigns. In each sampling campaign, about 1 kg of soil was collected from the surface layer of each point (0–5 cm of depth). The attributes (color, texture, structure, and gross elements content estimation) of each sample were recorded. This description was accompanied by a physicochemical analysis in the laboratory to determine properties such as EC (Table II).

TABLE I
COHERENCE IMAGERY PAIRS

Pair number	Date SLC1	Date SLC2	Mode of incidence	Incidence angle (°)
Pair 1	27 September 2011	21 October 2011	FQ7	25.7
Pair 2	21 October 2011	14 November 2011	FQ7	25.7
Pair 3	27 September 2011	14 November 2011	FQ7	25.7
Pair 4	20 October 2011	13 November 2011	FQ9	28
Pair 5	30 September 2011	24 October 2011	FQ25	43.6
Pair 1	27 September 2011	21 October 2011	FQ9	28
Pair 2	19 October 2011	21 November 2011	FQ16	35.4
Pair 3	23 October 2011	16 November 2011	FQ26	44.4
Pair 4	24 October 2011	17 November 2011	FQ26	44.4

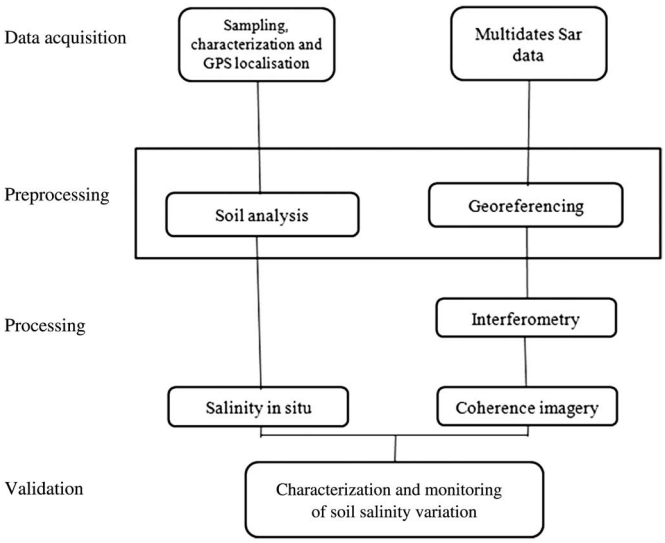

Fig. 3. Methodology used.

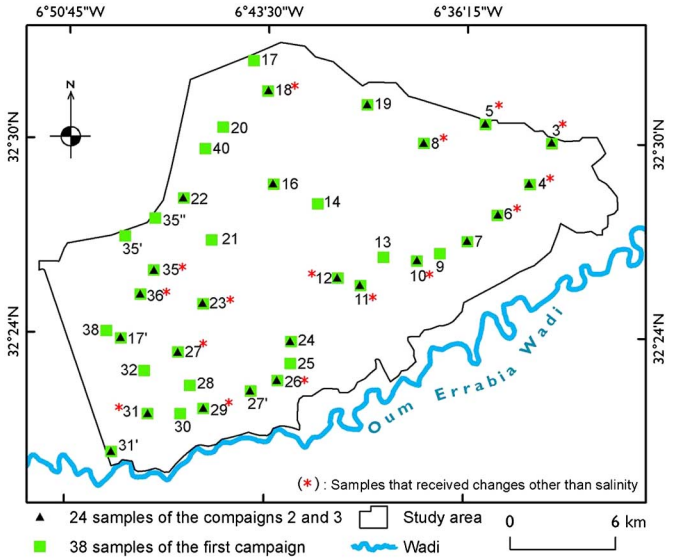

Fig. 4. Location of sampling points (Moroccan site).

B. InSAR Coherence Computation

The study focused on nine pairs of images, four pairs for the Moroccan site, and five pairs for the Tunisian site, corresponding to the following periods.

1) The end of the dry season (September).
2) The onset of autumn (October).
3) The onset of winter (November).

C. Coherence Map Generation

Fig. 6 shows the methodology used to establish a model linking variation in EC and interferometric coherence for the two study sites. We first attributed geographical coordinates to the SAR images using BEAM software. The projection used is on the Universal Transverse Mercator (UTM) geospatial reference system in the WGS84 geodesic system, zones 32 and 29 North, respectively, for the Tunisian and Moroccan sites.

1) Generate coherence image: we generated a coherence image for each of the different pairs and for each polarization (HH/HV/VV).
2) Coherence was calculated for 3×3 pixel windows. We averaged coherence over windows of 3×3 pixels, corresponding to 24 m $\times$ 24 m, to avoid registration and georeferencing errors.

D. EC Modeling With Respect to Coherence

Model calibration: Next, we developed general regression models to analyze the variation in EC (measured in situ) in relation to interferometric coherence (extracted from the radar image). For this exploratory study, we used simple linear regression models to determine the pattern of variation.

It should be noted that during the second and third campaigns, some changes occurred in the agricultural field due to the plowing by farmers. We eliminated the sampling points

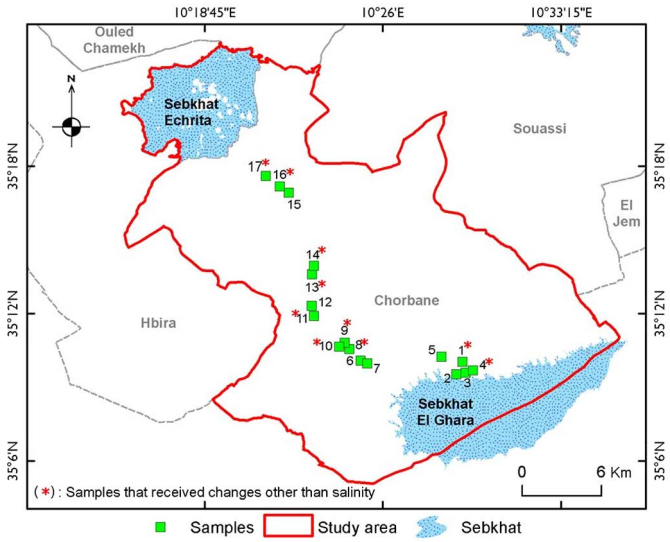

Fig. 5. Location of sampling points (Tunisian site).

TABLE II
DATE OF THE CAMPAIGN FOR EACH TEST SITE

Campaign	Tunisian site	Moroccan site
First campaign	September 26, 2011	September 27 and 28, 2011
Second campaign	October 24, 2011	October 24, 2011
Third campaign	November 17, 2011	November 17, 2011

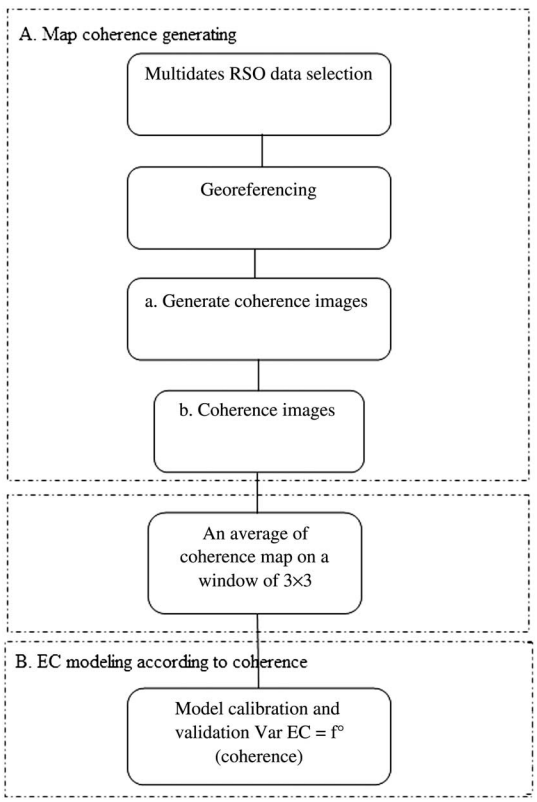

Fig. 6. Methodology used to establish model Var CE = f° (coherence).

TABLE III
TUNISIAN SITE SAMPLE CHARACTERISTICS

Land cover	Sampling
Olive	1, 6
Bare soil	2, 3, 4, 5, 7, 9, 12, 14, 15, 16
Weeds	8, 10, 11, 13, 17
Roughness changes	4, 8, 10, 11, 16, 17
Moisture	1, 9, 14, 13

TABLE IV
MOROCCAN SITE SAMPLE CHARACTERISTICS

Land cover	sampling
Bare soil	7, 6, 22, 23, 4, 29, 26, 16, 27, 31', 27', 10, 11
Weeds	3, 5, 17', 18, 5, 8, 24, 36, 31, 19
Crops	12, 3
Roughness changes	18, 23, 8, 4, 29, 31, 31', 10, 11
Moisture	35, 17', 6, 5, 12, 3, 26, 36, 27, 27'

where changes other than salinity occurred (Figs. 4 and 5). In Tables III and IV, we list the changes in each sampled plot (moisture, roughness, and vegetation cover) for the two sites.

1) Evaluation of the Models: To evaluate the performance of the models, we used four indices (coefficient of determination R^2, relative bias $BIAS_r$, relative root mean square error $RMSE_r$, and relative Nash–Sutcliffe efficiency Nr), and a confusion matrix analysis.

1) Coefficient of determination R^2 is defined as the squared value of the coefficient of correlation. It is calculated as [23]

$$R^2 = \left[\frac{\sum_{i=1}^{n} (O_i - O) * (ES_i - ES)}{\sqrt{(\sum_{i=1}^{n} (O_i - O)^2) * \sqrt{(\sum_{i=1}^{n} (ES_i - ES)^2)}} \right]^2. \quad (1)$$

The value of R^2 lies between 0 and 1. A value of zero means no correlation, whereas a value of 1 means that the dispersion of the prediction is equal to that of the observation [23].

2) $BIAS_r$ is calculated as

$$BIAS_r = \frac{1}{n} * \sum_{i=1}^{n} \left(\frac{ES - O_i}{ES_i} \right). \quad (2)$$

3) $RMSEr$ is a commonly used statistical measure of error. Generally, the lower the value of RMSEr, the better the performance of the model

$$RMSE_r = \sqrt{\frac{1}{n} * \sum_{i=1}^{n} \left(\frac{ES_i - O_i}{ES_i} \right)^2}. \quad (3)$$

TABLE V
MODEL PERFORMANCE' DETERMINATIONS (FIRST–SECOND CAMPAIGNS)

Model EC = f°(coherence)	R^2 calibration	R^2 cross validation	RMSE cross validation	Bias cross validation	Nash cross validation
HH (FQ7 Tunisia)	0.07	–0.27	251	–179	–0.35
HV (FQ7 Tunisia)	0.01	0.10	372	–413	–0.49
VV (FQ7 Tunisia)	0.07	–0.75	305	269	–0.71
HH (FQ9 Morocco)	0.21	0.08	311	–80	–0.69
HV (FQ9 Morocco)	0.25	0.03	100	–26	–0.69
VV (FQ9 Morocco)	0.20	0.09	386	–99	–0.68
HH (FQ26 Morocco)	0.004	0.01	270	–69	–0.99
HV (FQ26 Morocco)	0.068	0.04	621	–160	–0.44
VV (FQ26 Morocco)	0.052	0.07	609	–157	–0.99

4) The Nash–Sutcliffe statistic evaluates model performance by comparing the accuracy of estimated values to the observed mean value of the entire data set [27]

$$Nr = \frac{\sum_{i=1}^{n}\left(\frac{ES_i - O_i}{ES_i}\right)^2}{\sum_{i=1}^{n}\left(\frac{O_i - O}{O}\right)^2}. \quad (4)$$

where n is the sample size, O_i and Es_i are the observed and estimated values, and O and Es are the means of the observed and estimated values.

If the result is negative, the estimation is worse than using the mean value; the criterion is equal to one for a perfect estimation [24].

5) The confusion matrix compared the predicted classifications (using the InSAR coherence approach being assessed) and the real (measured through the field campaign) ones. The performance of such systems is evaluated using the data in the matrix [30]. Samples were classified in the confusion matrix into three classes according to salinity variation: low, medium, and high.

IV. EXPERIMENTAL RESULTS

A. Monitoring Soil Salinity During First and Campaigns

To monitor soil salinity variation between the first and second campaigns, we used HH, HV, and VV polarized coherence images with an incidence angle of 25.7° (September 27–October 21) for the Tunisian site and incidence angles of 28° (September 27–October 21) and 44.4° (September 30–October 24) for the Moroccan site. The objective was to examine the impact of these parameters. There was almost no correlation between EC variation and interferometric coherence for any of the three types of polarization. The coefficients of determination of the different models confirm that, between the two campaigns, EC variation was independent of interferometric coherence. This means that the salinity variation was not detected by the SAR signal. Cross-validation results confirmed the inefficiency of the SAR tool for soil salinity detection: R^2 was very low in all models, *Nash* values were negative, error was very high, and bias values indicate that the *EC* values were underestimated (Table V). In addition to the results of cross-validation, the confusion matrix showed that the percentage of samples that were well classified was low, confirming the nonperformance of the model.

A classification system was established to distinguish between low, medium, and high variation of salinity. The confusion matrix analyzed eight samples: six low, one medium, and one high variation sample, according to the onsite measurements. We can see from the matrix that the model had trouble distinguishing between low and medium variation. The majority of real classification samples were in the low variation class, but the majority of the predictions were in the medium class. When we examine the diagonal of the matrix, we note that only 12.5% of samples were well classified (Table VI). On the Moroccan site, the majority of real classifications were in the medium variation class but the majority of predicted classifications were in the high variation class. The inefficiency of the SAR tool in the measurement of EC could be explained by the low soil moisture content during this period. Indeed, the dielectric constant of the area is the determinant of the backscattered signal intensity. For all radar frequencies, moisture corresponds to an increase of the dielectric constant ε [12]. Thus, the greater the level of soil moisture, the more significant the effect of salinity will be on the imaginary part of the dielectric constant ε [12], [25], [26]. This is due to the solubility of salts in water. Since soil moisture is largely formed by rainfall, we decided to analyze the rainfall recorded in the two study sites during the field campaigns. Fig. 7 shows the diagram of rainfall. The acquisition of SAR images and field measurements during the first period coincided with an absence of rainfall, indicating low soil moisture. The first rain was recorded on the afternoon of October 25, 2011, just a few hours after image acquisition and soil sampling in the second campaign.

TABLE VI
CONFUSION MATRIX ASSESSMENTS (FIRST–SECOND CAMPAIGNS)

Polarization	Incidence angle (°)	% of correctly classified instances (matrix diagonal)
HH	25.7 (Tunisia)	25
	28 (Morrocco)	38.8
	44.4 (Morrocco)	38.8
HV	25.7 (Tunisia)	12.5
	28 (Morrocco)	38.8
	44.4 (Morrocco)	44.4
HV	25.7 (Tunisia)	12.5
	28 (Morrocco)	38.8
	44.4 (Morrocco)	44.4

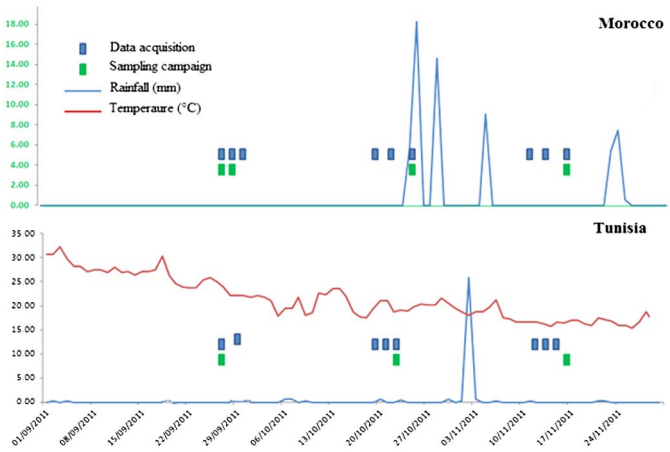

Fig. 7. Rainfall and temperature versus data acquisition's dates.

B. Monitoring Soil Salinity During Second and Third Campaigns

1) Tunisian Site: For the second and third campaigns, we used coherence images with incidence angles of 25.7°, 28°, and 43.6° and HH, HV, and VV polarizations. Figs. 8–10 represent the patterns established between change in the percentage of EC and InSAR coherence. For the incidence angle of 25.7°, the coefficient of determination was as high as 78% in the HH polarization. However, the HV and VV polarizations also produced acceptable results. We note that if the radar detects variation in moisture and/or roughness, the InSAR coherence variation should be very important (tends to lower values). However, examination of Fig. 10 shows that around 0.7 (high value of coherence), InSAR coherence variation is low and does not exceed 0.1 for a 20% variation of EC. This low variability of coherence shows that variation in factors other than salinity, i.e., moisture and roughness, did not have a significant effect.

For the incidence angle of 28°, the model has a very low coefficient of determination. So, for this incidence, the

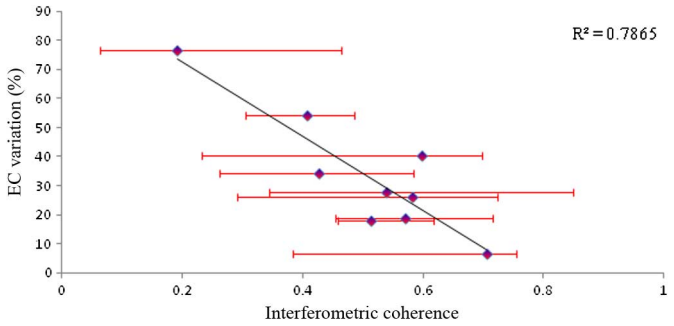

Fig. 8. Relationship between EC variation and interferometric coherence for second to third campaigns (21 October–14 November) with an incidence angle of 25.7° and HH polarization.

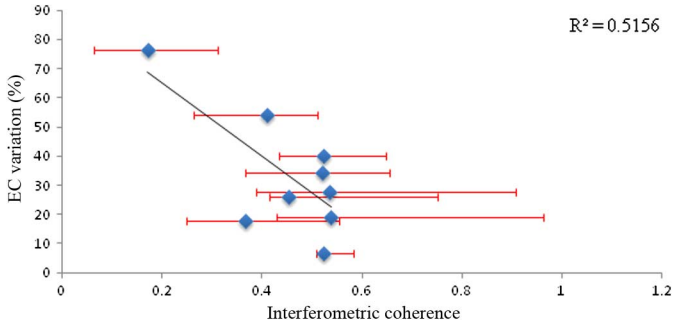

Fig. 9. Second to third campaigns (21 October–14 November) with an incidence angle of 25.7° and HV polarization.

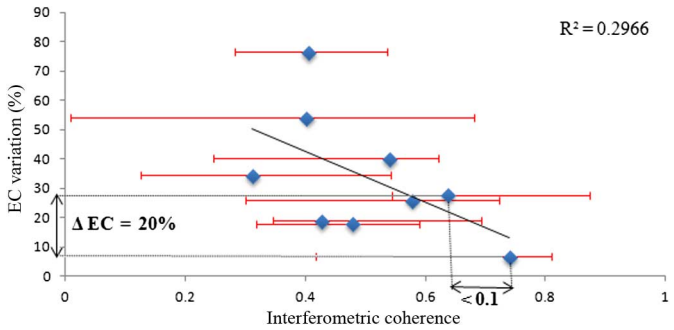

Fig. 10. Second to third campaigns (21 October–14 November) with an incidence angle of 25.7° and VV polarization.

coherence cannot explain the EC variation. However, the change that was detected by the SAR image could be explained by other biophysical parameters (roughness, moisture, etc). In addition, the 4-day time lag between the SAR image acquisition and the field campaigns (Image acquisition: October 20–November 13; measurements in situ: October 24–November 17) may have influenced the results. The model was also nonsignificant for the incidence angle of 43.6°. Table VII shows that only the first model (25.7° incidence angle; HH polarization) was acceptable, with an R^2 value of 0.68, *Nash* value of 0.67, and $RMSE_r$ of 48%. By contrast, the other models had lower R^2, negative *Nash*, and high $RMSE_r$ values. The results of the confusion matrix confirm these conclusions (Table VIII). For this campaign, the confusion matrix had nine samples: two low, five medium,

TABLE VII
MODEL PERFORMANCE' DETERMINATIONS (SECOND–THIRD CAMPAIGNS), TUNISIAN SITE

Model EC = $f°$ (coherence)	R^2 calibration	R^2 cross validation	RMSE cross validation	Bias cross validation	Nash cross validation
HH (FQ7)	0.78	0.68	48	–14	0.67
HV (FQ7)	0.51	0.071	65	–46	–0.17
VV (FQ7)	0.29	0.042	53	–1.52	–0.11
HH (FQ9)	0.04	0.31	83	–69	–0.52
HV (FQ9)	0.03	0.09	79	–73	–0.39
VV (FQ9)	0.0002	0.77	82	–70	–0.40
HH (FQ25)	0.13	0.16	80	–67	–0.43
HV (FQ25)	0.43	0.05	94	–46	–0.06
VV (FQ25)	0.20	0.0007	71	–53	–0.18

TABLE VIII
CONFUSION MATRIX ASSESSMENTS (SECOND–THIRD CAMPAIGNS), TUNISIAN SITE

Polarization	Incidence angle (°)	% of correctly classified instances (matrix diagonal)
HH	25.7	66.66
	28	33.3
	43.6	33.3
HV	25.7	44.4
	28	33.3
	43.6	55.5
HV	25.7	55.5
	28	44.4
	43.6	55.5

and two high variation samples, according to the onsite measurements. Predicted classifications included one low, four medium, and one high variation. samples, i.e., only three samples were not classified correctly. Interpretation of the matrix diagonal showed that the model with the 25.7° angle of incidence and HH polarization classified samples well 66.66% of the time.

2) Moroccan Site: To monitor salinity at the Moroccan site, between the second and third campaigns, we used coherence images taken at 35.4° (19 October–21 November) and 44.4° (24 October–17 November) angles of incidence with HH, HV, and VV polarization. For the incidence angle of 35.4°, the model had a very low coefficient of determination. Consequently, for this incidence angle the coherence cannot explain the EC variation. However, the change detected by

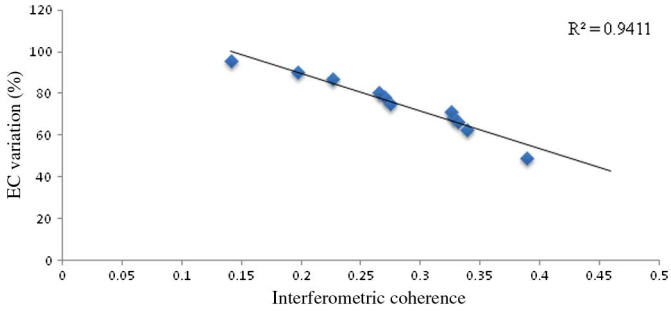

Fig. 11. Second to third campaigns (24 October–14 November) with an incidence angle of 44.4° Moroccan site.

the SAR image is explained by other biophysical parameters (roughness, moisture variation, etc.). For the incidence angle of 44.4°, on the other hand, EC variation corresponded well to the interferometric coherence fluctuation. The correlation was highly significant for cross-polarization (HV). The coefficients of determination confirm the strong relationship between the measured variables (more than 94%), as shown in Fig. 11; Table IX. The confusion matrix of the Moroccan site shows that, during the second and third campaign, 100% of the samples were well classified for the incidence angle of 44.4° and HV polarization. The samples of this campaign were classified in the high variation class for both the real and the predicted measures (11 samples in each case).

C. Monitoring Soil Salinity During the First and Third Campaigns

As with the second and third campaigns and first and second campaigns, we tried to establish a model relating EC variation and coherence between the first and the third campaigns. Fig. 12 shows the model calibration and cross-validation of the first and third campaigns for the 25.7° incidence angle and HH, HV, and VV polarizations. The first and third campaign looks only at the Tunisian site because SAR images of the Moroccan site were not available for the third campaign. The analysis of the different models illustrated on Fig. 12 shows that the model featuring HH polarization was the most acceptable because it had a coefficient of determination of 36%, whereas the HV model does not show any relationship between coherence and EC variation. This affirms that the results depend essentially on the polarization. Table X shows the results of cross-validation of the model, confirms these results and shows that only the model with an incidence angle of 25.7° and HH polarization was acceptable, with a RMSEr value of 36% and Nash value of 0.05. The confusion matrix shows that a low percentage of samples were well classified, indicating that the model performed poorly (Table XI). All eight of the samples were predicted to be in the high variation class. In fact, six samples were in the medium class, one was in the low class, and one was in the high class. We can see from the matrix that the model had trouble distinguishing between low, medium, and high salinity variation. The modeling of EC according to interferometric coherence shows that this relationship was mainly influenced by two parameters: 1) polarization and 2) incidence angle.

TABLE IX
MODELS PERFORMANCE DETERMINATIONS (SECOND–THIRD CAMPAIGNS), MOROCCAN SITE

Model EC = $f°$(coherence)	R^2 calibration	R^2 cross validation	RMSE cross validation	Bias cross validation	Nash cross validation
HH (FQ16)	0.004	0.005	125	–40	–0.64
HV (FQ16)	0.165	0.70	39	–7	0.11
VV (FQ16)	0.007	0.35	59	–23	–0.3
HH (FQ26)	0.227	0.31	83	70	–0.68
HV (FQ26)	0.941	0.74	70	–0.3	0.29
VV (FQ26)	0.0007	0.5	97	–0.3	–0.65

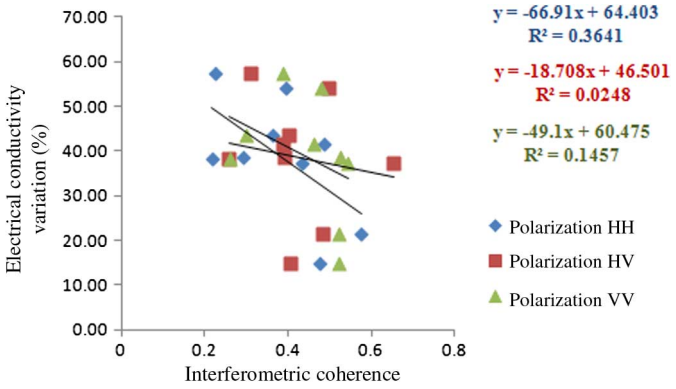

Fig. 12. Relationship between EC variation and coherence for first to third campaigns (27 September–14 November) with an incidence angle of 25.7° Moroccan site.

TABLE X
CROSS-VALIDATION OF MODEL PERFORMANCE (FIRST–THIRD CAMPAIGNS), TUNISIAN SITE

Evaluation model indices	HH FQ7	HV FQ7	VV FQ7
R^2	0.08	0.21	0.007
Nr	0.05	–1.06	–0.31
RMESr	36	42	40
BIASr	–13	–12	–19

TABLE XI
CONFUSION MATRIX ASSESSMENTS (FIRST–THIRD CAMPAIGNS)

Model EC = $f°$(coherence)	% of correctly classified instances (matrix diagonal)
HH (25.7°)	12.5
HV (25.7°)	12.5
VV (25.7°)	12.5

V. CONCLUSION

As mentioned above, this work sought to examine if the spatio-temporal dynamics of soil salinity could be detected by SAR. To answer this question, we applied several stages of processing to images of two sites, one in Morocco and one in Tunisia. The approach used was to consider the soil EC data point by point in a 3×3 pixel grid. This enabled us to develop a model to relate InSAR coherence to EC. In the case of the Tunisian site, the obtained results showed optimum estimation of salinity variation with HH and VV polarization and low incidence angles (25.7°). However, in Moroccan site, the SAR signal was more sensitive to EC variation at high incidence angles (44.4°) with HV polarization. This work provides some general indications of the best incidence angles and polarizations for modeling salinity from SAR data.

A. Polarization Effect

1) For the Tunisian site, the obtained results showed optimal estimation of EC according to interferometric coherence in the case of HH polarization (horizontal emission and reception). For low incidence angles like 25.7°, this model will provide more relevant information on the ground and vegetation compared to VV polarization (vertical emission and reception), which is sensitive to vertical objects.
2) For the Moroccan site, HV polarization was more sensitive to the EC variation than parallel polarization at the 44.4° incidence angle. According to [11], [12], cross-polarization acquisitions are efficient for the detection of water content, while the correlation between the high soil moisture during this period and soil salinity can explain the sensitivity of the HV polarization in this case.

B. Incidence Angle Effect

In the case of the Tunisian site, the optimum configuration for EC detection was a low incidence angle and HH polarization. By contrast, for the Moroccan site, the sensitivity of the SAR signal to EC variation was higher at the 44.4°

incidence angle and HV polarization. Due to the fact that the Moroccan site is agricultural, there was more roughness due to tillage at that site. In accordance with references [12], [13], an increase in surface roughness influences the intensity of the signal reflected back to the sensor, resulting in a clear appearance of the surface on the SAR image. That surface roughness is better perceived by the SAR sensor when the angle of incidence is high [12], [28].

On the other hand, at the Tunisian site, which did not contain rough, bare soil where salinity was mainly related to moisture, our results confirm those of other studies that show that the optimal configuration for the best sensitivity of the backscattering coefficient as a function of soil moisture combines HH polarization and a low incidence angle [12], [29].

Such results could be useful for future research on the use of interferometric data to monitor soil salinization. However, to obtain better results, several refinements must be considered. We recommend that future studies.

1) Increase the number of soil samples collected. In order to obtain better estimates, it is preferable that the sample size be as large as possible.
2) Quantify the roughness of the surface. The desired degree of accuracy cannot be achieved without a quantitative measure of this characteristic.
3) Test the "soil texture" in addition to its EC.
4) Use the same radar image configurations (incidence mode) for the other study sites.

REFERENCES

[1] IPTRID-FAO, *Conférence electronique sur la salinisation: Extension de la salinisation et Strategies de prévention et rehabilitation*, 2006, pp. 4–7.

[2] J. P. Legros, "La salinsation des terres dans le monde," in *Proc. Academie des Sciences et Lettres de Montpellier Conf. n 4069*, 2009, pp. 257–269.

[3] S. Antipolis, "Les menaces sur les sols dans les pays mediterraneens." *Plan bleu.* p. 80, 2003. ISBN: 2-912081-13-0 V 2.

[4] H. Maitre, *Processing of Synthetic Aperture Radar Images.* New York, NY, USA: Springer, 2007.

[5] J. A. Richards, *Remote Sensing With Imaging Radar*, Berlin, Germany: Springer-Verlag, 2009.

[6] M. Zribi, *Developpement de nouvelles methodes de modelisation de la rugosite pour la retrodiffusion hyperfrequence de la surface du sol., teledetection: Traitement du signal.* Toulouse, France: Universite Paul Sabatier, 1998.

[7] H. Maitre, *Processing of Synthetic Aperture Radar Images*. British Library Cataloguing-in-Publication Data, 2001. ISBN: 978-1-84821-024-0.

[8] N. Holah, "*Potentiel des nouveaux capteurs radar multipolarisation et polarimetrique pour la caracterisation des etats de surface en milieu agricole*," These presentee a l'universite d'Orleans, France, 2005, p. 247.

[9] F. T. Ulaby, P. P. Batlivala, and M. C. Dobson, "Microwave backscatter dependence on surface roughness, soil moisture and soil texture: Part 1—Bare soil," *IEEE Trans. Geosci. Remote Sens.*, vol. 16, no. 4, pp. 286–295, Oct. 1978.

[10] M. Zribi and M. Dechambre, "A new empirical model to retrieve soil moisture and roughness from C-band radar data," *Remote Sens. Environ.*, vol. 84, pp. 42–52, 2002.

[11] F. T. Ulaby, C. T. Allen, and G. Eger, "Relating the microwave backscattering coefficient to leaf area index, *Remote Sens. Environ.*, vol. 14, pp. 113–133, 1984.

[12] F. T. Ulaby, R. K. Moore, and A. K. Fung, *Microwave Remote Sensing, Active and Passive: Radar Remote Sensing and Surface Scattering and Emission Theory*. Reading, MA, USA: Addison-Wesley Publishing Company, 1986.

[13] A. K. Fung, Z. Li, and K. S. Chen, "Backscattering from a randomly rough dielectric surface," *IEEE Trans. Geosci. Remote Sens.*, vol. 30, no. 2, pp. 356–369, Mar. 1992.

[14] F. Demontoux, B. Le crom, G. Ruffié, J. P. Wigneron, J. P. Grant, and F. Heather Lawrence, Etude d'un modele d'inversion liant l'emissivite a l'humidite des sols. Contribution a la mise au point de l'algorithme de la mission SMOS, *TELECOM'2007 and JFMMA journées Franco-Maghrebines des Micro-ondes et de leurs Applications*, Fes, Maroc, 2007, p. 4.

[15] M. Zribi, A. Le Morvan, and N. Baghdadi, Dielectric constant modelling with soil-air composition and its effect on SAR radar signal backscattered over soil surface, *Sensors*, vol. 8, pp. 6810–6824, 2008.

[16] A. Chahbi, *Analyse et estimation de l'etat hydrique et de la salinite du sol sur la plaine de Kairouan par teledetection radar*, Memoire de mastere, Institut nationale agronomique de la Tunisie, Tunisia, 2010, p. 65.

[17] S. Paloscia, P. Pampaloni, S. Pettinato, and E. Santi, Generation of soil moisture maps from ENVISAT/ASAR images in mountainous areas: A case study, *Int. J. Remote Sens.*, vol. 31, no. 9, pp. 2265–2276, 2010.

[18] G. I. Metternicht, Fuzzy classification of JERS-1 SAR data: An evaluation of its performance for soil salinity mapping, *Ecol. Modell.*, vol. 111, pp. 61–74, 1998.

[19] Z. Aly, F. Bonn, and R. Magagi, Modeling the backscattering coefficient of salt affected soils: Application to Wadi el Natrun Bottom, Egypt, in *eProc. 3rd Workshop EARSeL*, 2004, pp. 372–381.

[20] M. Grissa, R. Abdelfattah, G. Mercier, M. Zribi, A. Chahbi, and Z. Lili-Chaabane, Empirical model for soil salinity mapping from SAR data, in *Proc. IEEE Int. Geosci. Remote Sens. Symp.*, 2011, pp. 1099–1102.

[21] F. Houcine, A. Hadoud, M. Belhadj-Aissa, M. Fekir, and A. Belhadj-Aissa, Methode de deroulement de phase interferometrique : Etude comparative et application, *Vers une maîtrise des impacts environnementaux de l'irrigation*, 2009, p. 6.

[22] A. Amari and M. Bedir, "Les bassins quaternaires du Sahel central de la Tunisie. Genese et evolution des sebkhas en contexte décrochant compressif et distensif," *Géodynamique*, vol. 4, no. 1, pp. 49–56, 1989.

[23] P. Krause, D. P. Boyle, and F. Bâse, Comparison of different efficiency criteria for hydrological model assessment, *Adv. Geosci.*, vol. 5, pp. 89–97, 2005.

[24] D. N. Moriasi *et al.*, Model evaluation guidelines for systematic quantification of accuracy in watershed simulation, *Amer. Soc. Agr. Biol. Eng.*, vol. 50, pp. 885–900, 2007.

[25] Y. Shao *et al.*, Effect of dielectric proprieties of moist salinized soils on backscattering coefficients extracted from radarsat image, *IEEE Trans. Geosci. Remote Sens.*, vol. 41, no. 8, pp. 1879–1888, Aug. 2003.

[26] J. Jenson, *Remote Sensing of the Environnement, an Earth Resource Perspective*, 2nd ed. Upper Saddle River, NJ, USA: Pearson Prentice Hall, 2007, p. 591.

[27] J. E. Nash and J. V. Sutcliffe, River flow forecasting through conceptual models: Part 1—A discussion of principals, *J. Hydrol.*, vol. 10, pp. 282–290, 1970.

[28] A. Beaudoin, Q. H. J. Gwyandn, and T. Le Toan, SAR observation and modeling of the Cbandbackscatter variability due to multi-scale geometry and soil moisture, *J. IEEE Trans. Geosci. Remote Sens.*, vol. 28, no. 5, pp. 886–894, Sep. 1990.

[29] N. Baghdadi, S. Gaultier, and C. King, Retrieving surface roughness and soil moisture from SAR data using neural network, *Can. J. Remote Sens.*, vol. 28, no. 5, pp. 701–711, 2002.

[30] F. Provost and R. Kohavi, On applied research in machine learning, *Mach. Learn.*, vol. 16, pp. 127–132, 1998.

Meriem Barbouchi received the engineering degree from the Institut National Agronomique de Tunisie (INAT), Tunis, Tunisia, in 2010, and the M.S. degree in sustainable management of natural resources from INAT, in 2012. Currently, she is pursuing the Ph.D. degree in desertification, environment and climate change in cooperation with INAT and COSIM (communication, signal, and image) Laboratory, Ecole Supérieur des Communication de Tunis (Sup'COM), Tunis, Tunisia.

Her research interests include remote sensing used in agriculture and environment.

Riadh Abdelfattah (SM'12) received the engineering degree from the École Supérieure des Postes et des Télécommunications (SUP'COM), Tunis, Tunisia, in 1995, the M.S. (DEA), and the Ph.D. degree in electrical engineering from the École Nationale Ingénieurs de Tunis, Tunis, Tunisia, in 1995 and 2000, respectively, and le Diplôme de l'Habilitation Universitaire from the Higher School of Communications (SUP'COM), University of Carthage, Carthage, Tunisia.

Between 2000 and 2002, he was a Postdoctoral Researcher with the Ecole Nationale des Télécommunications, Paris, France, consecutively with the Department TSI and then with the Department COMELEC. Currently, he is an Associate Professor with the Higher School of Communications for Engineers, University of Carthage, and an Associate Researcher with the Department ITI, Telecom-Bretagne, Institut de Telecom, Brest, France. He has authored and coauthored more than 60 journal papers, conference papers, and book chapter. His research interests include interferometric radar imagining, multitemporal and multiscale image analysis, desertification, flooding and soil salinity mapping from remote sensed data.

Dr. Abdelfattah is currently a member of the Executive Committee of the IEEE Tunisia Section (2013–2014).

Karem Chokmani received the B.Sc. degree in agricultural engineering from the Institut National Agronomique de Tunisie (INAT), Tunis, Tunisia, the M.Sc. degree in agriculture engineering from Laval University, Quebec, QC, Canada, and the Ph.D. degree in geomatics from Laval University.

He is a Professor of remote sensing and statistical hydrology at the INRS University, Montreal, QC, Canada. He joined the INRS-ETE in 2002 as a Postdoc, then as Research Associate, and now is a Professor. His research interests include development of remote sensing applications for spatiotemporal monitoring of water resources in a climatic change context. He also worked on the development of statistical tools for the local and regional estimation of hydrological variables.

Nadhira Ben Aissa photograph and biography not available at the time of publication

Rachid Lhissou was born in Tounfite, Morocco. He received the B.S. degree in geomatics from the Faculty of Sciences and Techniques of Beni-Mellal (FSTBM), Beni-Mellal, Morocco, in 2009, the M.S. degree in GIS from the Hassan II University, Casablanca, Morocco, in 2011. Currently, he is pursuing the Ph.D. degree working on soil salinity monitoring using SAR and optical remote sensing at FSTBM, Beni-Mellal, Morocco.

He is with the Team of Remote Sensing and GIS applied in Geosciences and Environment, Department of Earth Sciences, Faculté des Sciences et Techniques de Béni Mellal (FSTBM).

Abderrazak El Harti received the M.Sc. degree in geology and the Ph.D. degree in use of remote sensing and GIS in mineral exploration and geological mapping from the Cadi Ayyad University of Marrakech, Marrakesh, Morocco, in 1995 and 2005, respectively.

Currently, he is the Director of research team in remote sensing and GIS at the Sultan Moulay Slimane University, Beni-Mellal, Morocco. His research interests include the application of remote sensing and GIS to the mineral exploration and land degradation.